Growth kinetics of thin oxide layers; oxidation of Fe and Fe-N phases at room temperature

Kooi, Bart J.; Somers, Marcel A.J.; Mittemeijer, Eric J.

Published in:
Thin Solid Films

DOI:
10.1016/0040-6090(96)08682-8

Publication date:
1996

ELSEVIER

Thin Solid Films 281–282 (1996) 488–491

thin solid films

Growth kinetics of thin oxide layers; oxidation of Fe and Fe–N phases at room temperature

Bart J. Kooi [1], Marcel A.J. Somers *, Eric J. Mittemeijer

Delft University of Technology, Laboratory of Materials Science, Rotterdamseweg 137, NL-2628 AL Delft, The Netherlands

Abstract

The evolution of iron-oxide layers at room temperature on pure polycrystalline α-Fe and on the Fe–N phases γ-Fe[N], γ′-Fe_4N_{1-x} and ϵ-Fe_2N_{1-z} was followed in situ with Auger-Electron Spectroscopy. The observed oxidation kinetics of the Fe and Fe–N phases were interpreted using a model considering coupled fluxes of cations and (tunnelling) electrons and an electrostatic potential difference over the oxide layer changing during oxidation. It was concluded that the oxidation kinetics are largely controlled by cation transport governed by the chemical and electrostatic potential differences.

Keywords: Auger electron spectroscopy; Iron; Nitrides; Oxidation

1. Introduction

The atmospheric corrosion resistance of a ferritic workpiece can be improved by an oxidised iron-nitride layer composed typically of γ′-Fe_4N_{1-x} and/or ϵ-Fe_2N_{1-z} and iron oxide at the surface [1,2]. The mechanisms responsible for the improvement of the corrosion resistance are not understood. The present work aims at understanding the initial oxidation behaviour of Fe and Fe–N surfaces at room temperature.

2. Coupled currents model

During oxidation the transport of charged species through the oxide layer is determined by gradients of chemical and electrostatic potential [3–6]. In the coupled currents model [7] both cation and electron transport are considered in the direction parallel to the surface normal (z direction). Net transport of electric charge through the oxide layer is assumed not to occur [5,7]. The required balancing of cation and electron currents is realised by adaptation of the electrostatic field in the oxide.

Generally, the flux J_i of an ionic species i, under the influence of both a concentration gradient and a homogeneous electric field is given, in the steady-state approximation, by [6]:

$$J_i = 4a\nu \exp\left(-\frac{W}{kT}\right) \sinh\left(\frac{a}{\Lambda}\right)\left[\frac{C_L - C_0 \exp L/\Lambda}{1-\exp L/\Lambda}\right] \quad (1)$$

where $2a$ is the ionic jump distance, ν is the attempt frequency, W is the rate-limiting (activation) energy barrier, k is the Boltzmann constant, T is the temperature,

$$\Lambda^{-1} = \frac{Z_i e E_L}{kT}$$

where $Z_i e$ denotes the effective charge per particle of the ionic species during transport through the lattice [7], E_L is strength of the surface-charge field in the oxide determined by the surface concentration of charged oxygen, L is the instantaneous layer thickness and C_L and C_0 are concentrations of the diffusing species at oxide/oxygen ($z=L$) and at metal/oxide ($z=0$) interface, respectively. For the case of outward oxide-film growth, excess cations (in addition to some average cation concentration; see [7]) are assumed to be the diffusing species: $C_L < C_0$. The electrostatic potential difference over the oxide layer is given by $V = V_L - V_0 = -LE_L$. The value for E_L as a function of L is prescribed by the constraint of coupled charge currents [7,8]: $q_i J_i + q_e J_e = 0$ (q_i and q_e are the electric charges transported by ions and electrons and J_e is the electron flux). Equations describing J_e for the cases of electron transport by tunnelling through the potential barrier of the oxide layer and by thermionic emission were given in

* Corresponding author. Tel.: +31 15 278 2289; Fax: +31 15 278 6730; e-mail: somers@stm.tudelft.nl

[1] Now at: University of Groningen, Dept. Applied Physics, Materials Science Centre, Nijenborgh 4, NL-9747 AW Groningen, The Netherlands.

Refs. [7] and [8], respectively. The growth rate of a layer with thickness L follows from:

$$\frac{dL}{dt} = R_i J_i(L) \quad (2)$$

where R_i is the volume of oxide formed per single cation and $J_i(L)$ is the ionic flux for a film of thickness L.

Model calculations in [7] show that, for the case that electrons are transported by tunnelling, typically two-stages of growth kinetics for oxide films result: for $L \leq 2$ nm electron tunnelling proceeds rapidly and cation transport is rate limiting. Then, cation transport is promoted and electron tunnelling is impeded by negative charging of the surface. The maximum potential difference over the oxide layer, that is realised if no cation transport occurs, is the so-called Mott potential V_M at the surface: $V_M = (\chi_0 - \chi_L)/e$ (χ_0 and χ_L are the work functions at the substrate/oxide and the oxide/oxygen interface, respectively). For thicker films, electron tunnelling becomes rate limiting. Then, cation transport is impeded and electron tunnelling is promoted by positive charging of the surface.

3. Experimental

Polycrystalline pure α-Fe samples (impurities < 100 ppm) were studied in both 80% cold-rolled condition as well as in recrystallized condition. Polycrystalline surface layers of Fe–N phases were obtained by reaction diffusion of nitrogen, supplied by an NH_3/H_2 gas mixture, into an α-Fe substrate (impurities < 300 ppm). The Fe–N phase samples comprise:

- γ-Fe[N] (austenite): ~9 at.% N at the surface
- γ′-Fe_4N_{1-x}: 19.8 at.% N at the surface
- ϵ-Fe_2N_{1-z}: 27.1 at.% N at the surface

A Perkin–Elmer PHI 4300 Scanning Auger Microprobe (base pressure $< 7 \times 10^{-8}$ Pa) was used for in situ investigation of the oxidation behaviour of Fe and Fe–N phases. Each specimen surface was sputter cleaned prior to oxidation with 3.5 keV Ar^+ ions during 20 min and, subsequently, with 2 keV Ar^+ ions during 10 min, applying rotation. No annealing treatment was performed after sputter cleaning to prevent different crystal sublattices of the Fe and Fe–N phases from obscuring the role of nitrogen on the oxidation behaviour of iron atoms. Room temperature oxidation was carried out in 8.0×10^{-6} Pa O_2 total pressure. During oxidising a primary electron beam operated at 5 kV and 2 μA (beam diameter ~ 1 μm) was rastered over an area of 250×250 μm^2 of the specimen surface to obtain an average over several crystal orientations. Fe–$M_{2,3}VV$, N–$KL_{2,3}L_{2,3}$, O–$KL_{2,3}L_{2,3}$ and Fe–$L_{2,3}M_{4,5}M_{4,5}$ Auger transitions were monitored continuously in various experiments for each sample. Auger intensities were evaluated as peak-area-to-background-area ratios. Reproducibility of the resulting kinetic curves at several locations of the sample surfaces was found to be excellent. The influence of the incident electron beam on the oxidation kinetics was described elsewhere as well as further experimental details and considerations [10]. The thickness of the developing oxide-layers was calculated from the evolution of the O–$KL_{2,3}L_{2,3}$ intensities by comparison with the O–$KL_{2,3}L_{2,3}$ intensity of an "infinitely" thick layer of α-Fe_2O_3, assuming a homogeneous oxide layer with uniform thickness on the oxidising surface [9].

4. Results and discussion

The evolutions of the oxide-layer thickness during room-temperature oxidation of Fe and Fe–N phases at 8.0×10^{-6} Pa are shown in Fig. 1a. From the evolution of the N–KLL intensity, it was concluded that nitrogen from the Fe–N phases is not incorporated in the oxide layer, but buried underneath.

The coupled currents model for the case of cation transport and electron tunnelling [7], was fitted by a least squares fitting procedure to each experimental curve of oxide-layer

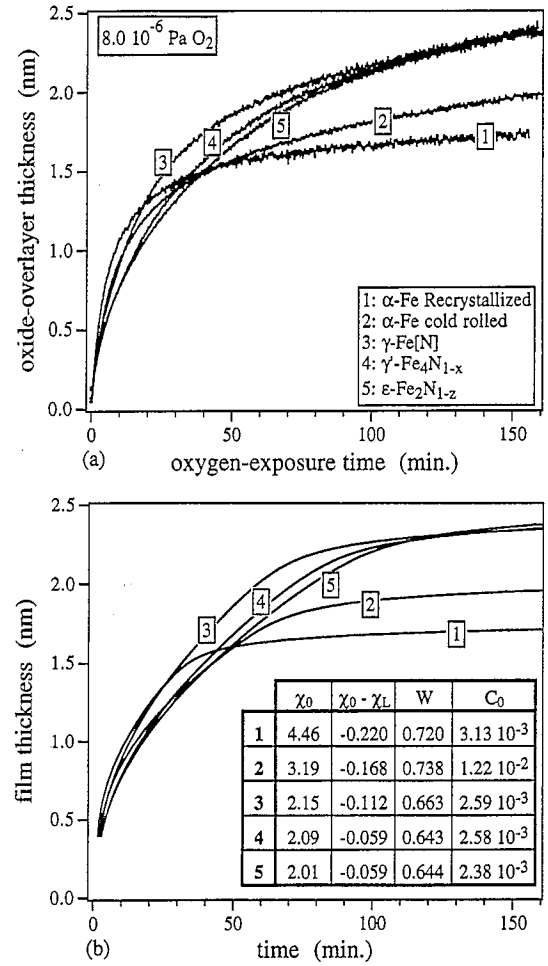

	χ_0	$\chi_0 - \chi_L$	W	C_0
1	4.46	-0.220	0.720	3.13 10^{-3}
2	3.19	-0.168	0.738	1.22 10^{-2}
3	2.15	-0.112	0.663	2.59 10^{-3}
4	2.09	-0.059	0.643	2.58 10^{-3}
5	2.01	-0.059	0.644	2.38 10^{-3}

Fig. 1. (a) Oxide-overlayer thickness as a function of oxidation time in O_2 at 8.0×10^{-6} Pa at room temperature for the polycrystalline α-Fe (recrystallized and cold rolled), γ-Fe[N], γ′-Fe_4N_{1-x} and ϵ-Fe_2N_{1-z} substrates. (b) Film thickness as a function of time as obtained by fitting Eq. (1) and tunnel equations provided in [7] to the experimental results in Fig. 1a. Values for parameters belonging to the curves are given in the table (χ_L, χ_0 and W in eV and C_0 in nm^{-3}). The values chosen for the other parameters were: $C_L = 10^{-3}$ nm^{-3}, $\nu = 10^{12}$ s^{-1}, $R_i = 0.016$ nm^3, $2a = 0.2968$, $Z = 3$.

thickness vs. oxidation time. The values for the work functions at the substrate/oxide and oxide/oxygen interface χ_0 and χ_L, respectively and W and C_0 (Eq. (1)) were taken as fitting parameters (for details of fitting procedure see [10]); the values of parameters taken constant in the calculations are gathered in the caption of Fig. 1b. The results obtained are shown in Fig. 1b. Sensitive fitting parameters appeared to be the work functions χ_0 and χ_L. The Mott potential ($V_M = (\chi_0 - \chi_L)/e$) becomes less negative in the order recrystallized α-Fe → cold-rolled α-Fe → γ-Fe[N] → γ′-Fe_4N_{1-x} → ϵ-Fe_2N_{1-z}, which appears to be realised by a decrease of χ_0 concurrent with a somewhat stronger decrease of χ_L (see Fig. 1b). The bulk concentrations of excess cations, C_0, (Fig. 1b) do not vary much, except for cold rolled α-Fe, where C_0 is higher.

A discrepancy is observed between fitted and experimental oxidation curves in the stage where electron tunnelling would be largely rate limiting: the calculated oxidation rate is significantly smaller than the experimental (compare Fig. 1a and 1b). Apparently, the actual net electron flux is larger than can be accounted for by tunnelling of electrons through the oxide layer. This may be due to the contribution of other mechanisms of electron transport. At room temperature the contribution of thermionic emission to electron transport is negligible for the film thickness regime and values of χ_0 considered [8]. Alternatively, transport of cations may still be largely rate determining in an advanced stage of oxidation. Consequently, a higher oxidation rate occurs than for the case electron tunnelling is largely rate determining. Nevertheless, the transports of cations and electrons have become more competitive in an advanced stage. Then, it is conceivable that the density of negatively charged oxygen anions at the surface, decreases more strongly than would be allowed to maintain the value of V (see below Eq. (1)). Hence, a model description in which V varies with oxidation time suggests itself.

The change of V with oxidation time was assessed by fitting Eq. (1) for cation transport to the experimental oxidation curves. This can be performed irrespective of the mechanism of electron transport. Results for the variation of V obtained from the growth kinetics of oxide layers on recrystallized α-Fe, γ-Fe[N], γ′-Fe_4N_{1-x}, and ϵ-Fe_2N_{1-z} as depicted in Fig. 1a, are presented in Fig. 2. In the fitting, apart from V and C_0, all parameters used in the flux equation for cation transport were taken constant ($W = 0.66$ eV an average of the values in Fig. 1b; see caption to Fig. 1b for the other values). The concentration of excess cations at the substrate/oxide interface, C_0, was chosen such, that V becomes approximately zero for the longest oxidation times (cf. Fig. 2). Taking $V \to 0$ on prolonged oxidation implies that, eventually, cation transport through the oxide layer becomes governed only by the chemical potential gradient.

The evolution of $|V|$, an initially steep increase followed by a shallow decline, can be interpreted qualitatively as follows. The initial increase of $|V|$ is ascribed to the chemisorption stage and the development of an isolating oxide layer

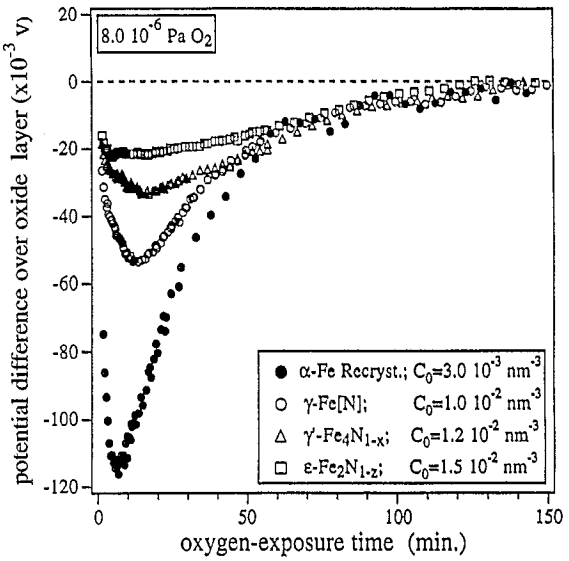

Fig. 2. Electrostatic potential difference over the oxide layer, V, as a function of oxidation time in O_2 at 8.0×10^{-6} Pa at room temperature for polycrystalline recrystallized α-Fe, γ-Fe[N], γ″-Fe_4N_{1-x} and ϵ-Fe_2N_{1-z} substrates as obtained by fitting the cation-flux equation (Eq. (1)) to the experimental results shown in Fig. 1a.

at the substrate surface, which are associated with strong changes of the work functions. The two interfaces metal/oxide and oxide/oxygen develop in this stage. The subsequent decline of $|V|$ is ascribed to a gradual reduction of the density of negatively charged oxygen at the surface.

For α-Fe, γ-Fe[N] and γ′-Fe_4N_{1-x} the maximum value for $|V|$ occurs at a film thickness of about 1 nm, which would correspond to about 3–4 monolayers of oxygen anions. The maximum value of $|V|$ is strongly related to the nitrogen content in the substrate: a higher nitrogen content corresponds to a lower maximum value for $|V|$. This observation parallels the trend observed for the absolute value of the Mott potential in Fig. 1b (table) and indicates that the transfer of an electron from the substrate to the adsorbate is facilitated by the presence of nitrogen.

The value of C_0 obtained on fitting increases in the order α-Fe recrystallized → γ-Fe[N] → γ′-Fe_4N_{1-x} → ϵ-Fe_2N_{1-z} (cf. legend in Fig. 2). Consequently, the driving force for cation diffusion increases with increasing nitrogen content of the substrate.

5. Conclusion

Experimental growth kinetics of the oxide layer on α-Fe, γ-Fe[N], γ′-Fe_4N_{1-x} and ϵ-Fe_2N_{1-z} could be described satisfactorily by a model assuming coupled currents of cations and electrons through the oxide layer, with a potential difference over the oxide layer that changes during oxidation. Antagonistic dependencies on nitrogen content of the two driving forces for the transport of the cations may explain the observed oxidation kinetics: (i) for initial oxidation an increase of oxidation rate with decrease of the nitrogen content at the surface due to a more negative electrostatic poten-

tial difference and (ii) for prolonged oxidation an increase of oxidation rate with increase of nitrogen content due to an increase of excess cation concentration at the substrate/oxide interface.

Acknowledgements

The authors are grateful to Ir. Willem Sloof and Ing. Elke Fakkeldij for the provision of Auger facilities and experimental assistance. Ir. Peter Graat is thanked for critical reading of the manuscript. These investigations have been supported financially by the Foundation for Fundamental Research of Matter (FOM), the Netherlands Technology Foundation (STW) and IOP-Metalen.

References

[1] K. Sachs and D.B. Clayton, *Heat Treat. Met., 6* (1979) 29.
[2] B. De Benedetti and E. Angelini, in Niku-Lari (ed.), *Advances in Surface Treatments*, Vol. 5, Pergamon Press, Oxford, 1987, p. 3.
[3] F.P. Fehlner and N.F. Mott, *Oxid. of Metals, 2* (1970) 59.
[4] M.J. Dignam, D.J. Young and D.G.W. Goad, *J. Phys. Chem. Solids, 34* (1973) 1227.
[5] W.W. Schmeltzer and D.J. Young, *Prog. Solid-State Chem., 10* (1975) 17.
[6] A.T. Fromhold and E.L. Cook, *J. Appl. Phys., 38* (1967) 1564.
[7] A.T. Fromhold and E.L. Cook, *Phys. Rev., 158* (1967) 600.
[8] A.T. Fromhold and E.L. Cook, *Phys. Rev., 163* (1967) 650.
[9] M.P. Seah, in D. Briggs and M.P. Seah (eds.), *Practical Surface Analysis*, Vol. 1, Wiley, Chichester, 1990, p. 201.
[10] B.J. Kooi, *Ph.D. Thesis,* Delft University of Technology, 1995.